

First detection of hotspot advance in a Compact Symmetric Object

Evidence for a class of very young extragalactic radio sources

I.Owsianik¹ and J.E.Conway²

¹ Toruń Centre for Astronomy, Radio Astronomy Dep. ul.Gagarina 11, 87-100 Toruń, Poland
e-mail iza@astro.uni.torun.pl

² Onsala Space Observatory, S-439 92 Onsala, Sweden,
e-mail: jconway@oso.chalmers.se

Received month day, year; accepted month day, year

Abstract. We present the results of multi-epoch global VLBI observations of the Compact Symmetric Object (CSO), 0710+439 at 5 GHz. Analysis of data spread over 13 years shows strong evidence for an increase in the separation of the outer components at a rate of $0.244 \pm 0.027 h^{-1}c$. Given an overall size of $101.5 h^{-1}pc$ this implies a kinematic age of only 1400 ± 150 yrs. This result strongly supports the idea that Compact Symmetric Objects are very young radio-loud sources. Furthermore the large radiative efficiency we calculate for 0710+439 is consistent with strong negative luminosity evolution and with CSO's evolving into classical double sources.

Given the observed hotspot advance in 0710+439 ram pressure arguments imply that the external density is 3cm^{-3} which is consistent with other estimates for CSO's and with the intercloud medium of Narrow Line Regions. Since the two hotspots in 0710+439 lie at similar distances from the core their mean advance speeds over the lifetime of the source must be the same (i.e approximately $0.122 \pm 0.014 h^{-1}c$). In contrast we find evidence that at present the advance speed of the Northern hotspot might be significantly larger than that of the Southern hotspot. Such a short term asymmetry can be explained by temporary interactions with NLR clouds or, as we consider more likely, it could be due to hydrodynamic instabilities which are predicted by 3D numerical simulations.

Key words: Radio Continuum: Galaxies — Galaxies:jets — Galaxies: active—galaxies: individual: 0710+439

1. Introduction

Most strong, compact ($< 1''$) radio sources when mapped at high resolution have a core-jet morphology, consisting of a bright unresolved core and a one-sided jet in which superluminal motion is often observed. These core-jet sources are thought to be due to the bases of relativistically beamed jets orientated close to the line of sight. However Phillips & Mutel (1982) first identified compact objects which appeared to be dominated by unbeamed emission and called them 'Compact Doubles'. Wilkinson et al. (1994) first termed this class of radio sources 'Compact Symmetric Objects' (CSO's) emphasising their primary property of symmetry. Characteristically these objects show high luminosity radio emission regions separated by $< 1\text{kpc}$ which are located symmetrically on both sides of the centre of activity. It is thought that these high brightness regions are due to hotspots and minilobes created by the termination of oppositely directed jets and that this emission is free from relativistic beaming effects.

From the earliest papers it was suggested that CSO's were young sources (Phillips & Mutel 1982), which evolved into larger-sized sources. Alternatively it has been proposed that CSO's are 'frustrated' sources, in which higher density and/or turbulence in the interstellar medium inhibits their growth to larger dimensions (van Breugel et al. 1984). Finally it has been proposed that they are a separate class of short lived objects, which 'fizzle out' after about 10^4 yrs and do not grow to large sizes objects (Readhead et al. 1994).

Detailed theories of the youth model of compact sources show that it is feasible that CSO's are part of an evolutionary sequence in which they later evolve into the slightly larger Compact Symmetric Sources (CSS), which finally evolve into classical doubles (Fanti et al. 1995,

Table 1. Journal of 5 GHz global VLBI observations of 0710+439

Epoch	1980.53	1982.93	1986.89	1989.73	1993.44
Duration (hr)	11	12	4 \times 1	10	4 \times 0.6
Antennas ^a	BKGFo	BKGFo	SjBWKGFYo	SBWjKGFPkY	BLSWjNgROPHIY
Maximum baseline (M λ)	136	136	136	138	146

^a S—26 m, Onsala Space Observatory, Onsala, Sweden; j—26 m, MkII Telescope, Jodrell Bank, Cheshire, U.K.; B—100 m, Max-Planck-Institute für Radioastronomie, Effelsberg, Germany; W—Westerbork Synthesis Radio Telescope, the Netherlands; K—36.6 m, Haystack Observatory of the Northeast Radio Observatory Corporation, Westford, MA; G—42.7 m, National Radio Astronomy Observatory, Green Bank, WV; F—26 m, George R. Agassiz Station of Harvard University, Fort Davis, TX; Y—26 m, VLA, Socorro, NM; o—40 m, Owens Valley Radio Observatory of the California Institute of Technology, Big Pine, CA; L—32 m, Istituto di Radioastronomia, Medicina, Italy; N—32 m, Istituto di Radioastronomia, Noto, Italy; g—22 m, Simeiz, Ukraine; k—25 m, VLBA antenna, Kitt Peak, AZ; R—25 m, VLBA antenna, Brewster, WA; O—25 m, VLBA antenna, Owens Valley, CA; P—25 m, VLBA antenna, Pie Town, NM; H—25 m, VLBA antenna, Hancock, NH; I—25 m, VLBA antenna, N. Liberty, IA;

Readhead et al. 1996b). De Young (1996) and Begelman (1996) have used simple physical models to confirm that CSO sources are probably not frustrated and confined but instead evolving. An obvious way to distinguish between competing models is to try to measure or set limits on the growth in overall size of CSO's and so determine their ages directly, which is the purpose of this paper.

2. General Source Properties

2.1. Optical properties

The radio source 0710+439 has been identified (Peacock et al. 1981) with a galaxy of r magnitude of 19.7 ± 0.2 . The emission-line redshift of the galaxy is $z = 0.518$ (Lawrence et al. 1996). At this redshift $1 \text{ mas} = 3.5 \text{ } h^{-1} \text{ pc}$ assuming $H_0 = 100 \text{ } h \text{ km s}^{-1} \text{ Mpc}^{-1}$ and $q_0 = 0.5$. The optical spectrum (Lawrence et al. 1996) shows absorption lines characteristic of an evolved stellar population and an optical continuum shape typical of an elliptical galaxy without any evidence for a nonstellar component.

2.2. Radio properties

0710+439 has high radio luminosity ($L_{5\text{GHz}} = 5 \times 10^{33} h^{-2} \text{ erg s}^{-1} \text{ Hz}^{-1}$; Wilkinson et al. 1994). The flux density is very weakly polarised ($< 0.15\% \pm 0.11\%$ at 5 GHz) and the observed variations of the flux are not statistically significant (Aller et al. 1992). The total angular size of the source is 29 mas, which corresponds to a projected linear size of $101.5 \text{ } h^{-1} \text{ pc}$. The source has been mapped by VLBI at several frequencies i.e. 1.6, 5, 10.7, and 15 GHz. These observations showed the overall triple structure of the source. Despite having three components this source was provisionally classified as a compact double based on the fact that more than 80% of the emission came from two almost equally bright components (Pearson & Readhead 1988). Conway et al. (1992) argued that the two outer components were hotspots and minilobes,

while the centre of activity was associated with the middle component, based on its compactness, spectrum and weak flux density variability. Recent multi-frequency observations (Taylor et al. 1996) reveal a compact component with a strongly inverted spectrum at the southern end of the middle component, suggesting that the true centre of activity lies there.

3. Observations and imaging

3.1. Observations

While at most frequencies 0710+439 has only been observed once, at 5GHz it has been observed with a global VLBI array at 5 epochs spread fairly evenly over a period of 13 years (see Table 1). The first three epochs were analysed by Conway et al. (1992). Here we reanalyse these first three epochs and add new data from two additional epochs; a global 10 station long track observation made on 25th September 1989 and a multi-snapshot 13 station global observation made on 11th June 1993.

3.2. Data reduction

Observations in all epochs were made in left circular polarisation (IEEE convention) and a bandwidth of 2 MHz was recorded using the MkII recording system (Clark 1973). The data were cross-correlated with the JPL-Caltech VLBI Processor. The data were fringe-fitted in AIPS (Schwab & Cotton 1983) and averaged to 1 minute; error bars for the averaged data were estimated from the internal scatter of the data over the averaging interval. Amplitude calibration (Cohen 1975) for each antenna was derived from measurements of the antenna gain and system temperature during the observations.

After amplitude calibration the data were edited and mapped using IMAGR (AIPS package 1995) and Difmap (Shepherd et al. 1994, 1995). Many iterations of phase self-calibration were performed before applying amplitude

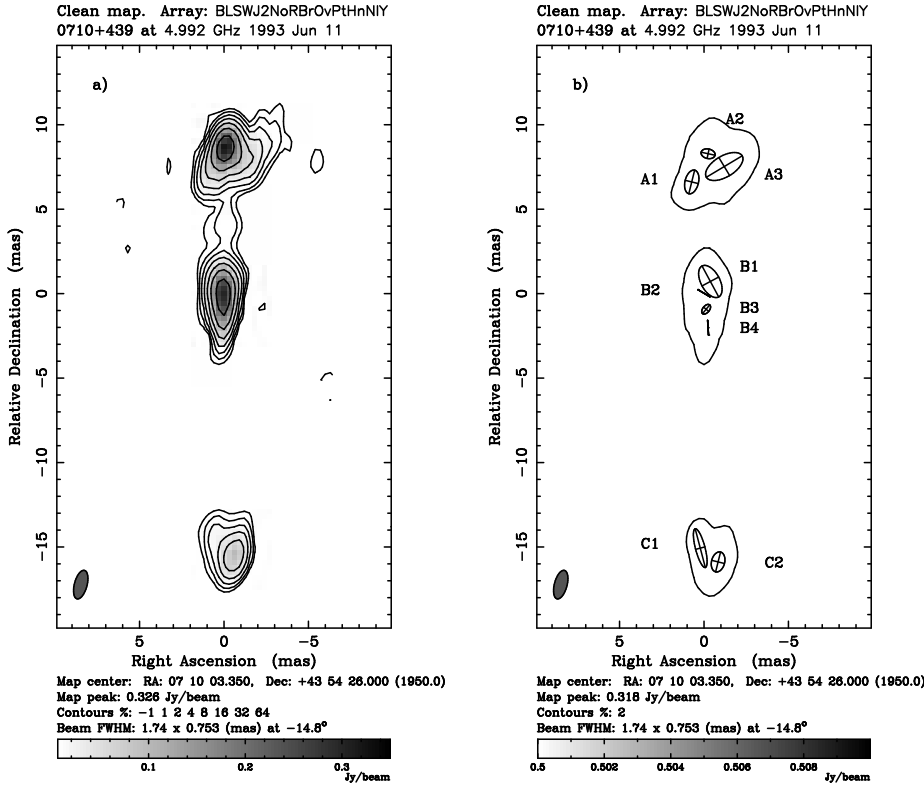


Fig. 1. (a) Fifth epoch map of 0710+439; (b) Diagram with position and size of the Gaussian model fit components.

self-calibration at the end. Windows for clean components were added to provide support and reject sidelobes. Initially each epoch was mapped separately starting with a point source model. The fitted restoring beams at each epoch were typically 1mas in the East-West direction and 1.5mas in the North-South direction. The highest dynamic range image was obtained from the 5th epoch data set (see Fig. 1a). Given this best map we therefore remade maps at all epochs using it as the starting model for self-calibration. As described in a Section 4 we then used these images to detect or set limits on internal motions within 0710+439.

Modelfitting with gaussian components was also carried out to the visibility data at each epoch using the program MODELFIT in the Caltech VLBI package (Pearson 1988), which fits to the amplitudes and closure phases directly and also with the gaussian modelfitting option within Difmap. The latter fits amplitudes and phases but allows phase self-calibration against the model, so that the model can converge to fit the closure phases. In all cases it was possible to obtain good fits to the data using only a few Gaussian components. The modelfitting process was started using gaussian components fitted to the 5th epoch CLEAN map using the AIPS task JMFIT. After varying all the gaussian parameters the best fitting model to the

fifth epoch data contained 9 components (see Fig. 1b, Table 2). This model provided a good fit with reduced Chi-squared agreement factor for amplitude $Q_{AMP}=1.258$ and for closure-phases $Q_{CLP}=1.180$ (for definition of agreement factor see Henstock et al. 1995). To characterise temporal changes in the source we obtained fits to the data at each epoch, using this 5th epoch model as a starting point (see section 4.1).

3.3. Source structure

The CLEAN map of the 5th epoch data (rms noise = 0.9 mJy beam⁻¹) shows clearly the overall triple structure of the source (see Fig. 1a). Maps at each epoch show three main components which we name (from North to South) A, B and C. Each of these main components shows substructure which is represented in the modelfits as separate gaussians (e.g. A1, A2 and A3; see Fig. 1b).

The CLEAN maps show that the Northern component (A) and the Southern (C) components show some faint extended emission around them. In addition to this both modelfitting and imaging indicate a compact feature (A2) within component A which we interpret (see Section 5.1) as a hotspot. The CLEAN images suggest a weak bridge of emission between A and the middle component B, how-

Table 2. Model for the 5th epoch of 0710+439

Components	S (Jy)	r (mas)	Θ ($^{\circ}$)	a (mas)	b/a	Φ ($^{\circ}$)
A1...	0.0694	6.6543	6.2614	1.4388	0.55597	-13.9796
A2...	0.4779	8.2871	-1.6703	0.8397	0.6750	77.7639
A3...	0.2507	7.6227	-9.0462	2.4721	0.50397	120.8770
B1...	0.0933	0.8137	-27.5533	2.0809	0.53689	28.2747
B2...	0.2737	0.0277	15.5553	0.8305	0.0033	59.2536
B3...	0.2141	0.9319	-172.195	0.6685	0.59546	-39.6004
B4...	0.1439	2.0326	-173.202	0.8779	0.00001	3.6030
C1...	0.0486	15.0697	179.154	2.3699	0.23898	14.6599
C2...	0.1531	15.9074	-176.993	1.2097	0.6450	166.0700

Parameters of the Gaussians components: S—flux density; r, Θ —polar coordinates, with polar angle measured from the north trough east; a, b—major and minor axes of the FWHM contour; Φ —position angle of the major axis measured from the north trough east.

ever imaging simulations show that this feature may not be reliable (see Appendix). We were not able to detect a similar jet-like feature connecting the middle and Southern components, which was found on a 1.6 GHz map (Xu 1994), possibly due to lack of surface brightness sensitivity. We were also not able to detect any emission located to the East of the C component, which is seen on the maps made by Wilkinson et al. (1994).

Fitting the B component required 4 gaussian subcomponents. Fig. 2a,b shows these gaussians as fitted to the 1st and 5th epochs respectively (convolved with a circular restoring beam of FWHM 0.7 mas). These images show that the B component is narrow at the South and becomes wider to the North. There also appears to be a slight kink in the jet with the major axis of the B3 component inclined at 45° with respect to the B2-B4 direction. A similar kink is seen in the 15 GHz maps and models (Taylor et al. 1996). Despite being separated by almost 13 years the model components for 5 GHz epochs 1 and 5 are very similar. One possible change is in the size of B1, however we conclude based on our imaging simulations that this may be an imaging artifact. In Section 4 we describe our detailed analysis of the multi-epoch data which shows components B2 and B4 to be stationary relative to each other, with a possible small northward motion of B3.

Overall our maps and modelfits to B agree closely with those estimated at 15 GHz by Taylor et al. (1996). However in our modelfits we did not require a compact component at the position of the core seen at 15 GHz. This is not unexpected given that at high frequency this component has a self-absorbed spectral index of $\alpha = 1.6 \pm 0.4$ (Taylor et al. 1996), where flux density $S \propto \nu^{\alpha}$. At 4.9 GHz with this spectral index we would expect the core to have a flux density of between 4.8 mJy and 11.8 mJy. At the position of the 15 GHz core on our 5th epoch super-resolved

map (0.5 mas FWHM, not shown) we did see a component with flux density 4.3 ± 1 mJy, if this feature is real it implies a spectral index of 2.1 ± 0.2 between 4.9 GHz and 15 GHz consistent with a synchrotron self-absorbed core component.

4. Multi-Epoch Intercomparison

4.1. Procedure

A serious problem with analysing data from VLBI observations is that there is significant freedom in making images. Data are degraded by instrumental errors, incomplete and different aperture coverages, and ambiguities in deconvolution and self-calibration. This can strongly affect the final results. For this reason intercomparison of models and maps made separately at each epoch is not a very good method of detecting small changes in a source (Conway et al. 1992).

To minimise the above effects we used the 5th epoch model and CLEAN map (see Fig. 1a,b) as starting points in re-modelfitting and re-mapping all of the epochs. This method should limit the differences between the final images of all five epochs of 0710+439, so we can be sure that any differences seen are demanded by the data and are due to real changes in the structure of the source (see Appendix).

The detailed procedure in modelfitting at each epoch was, starting with the 5th epoch model, to first allow just the flux density of all components to vary; however in each case the fit remained poor. We next allowed changes of all parameters of the gaussians within the B component (e.g. flux, radius, Θ , major axis, axis ratio, and Φ) which gave a somewhat better fit, but only after allowing all the components to move in position (which led to significant motion mainly in component A2) did we get a good fit.

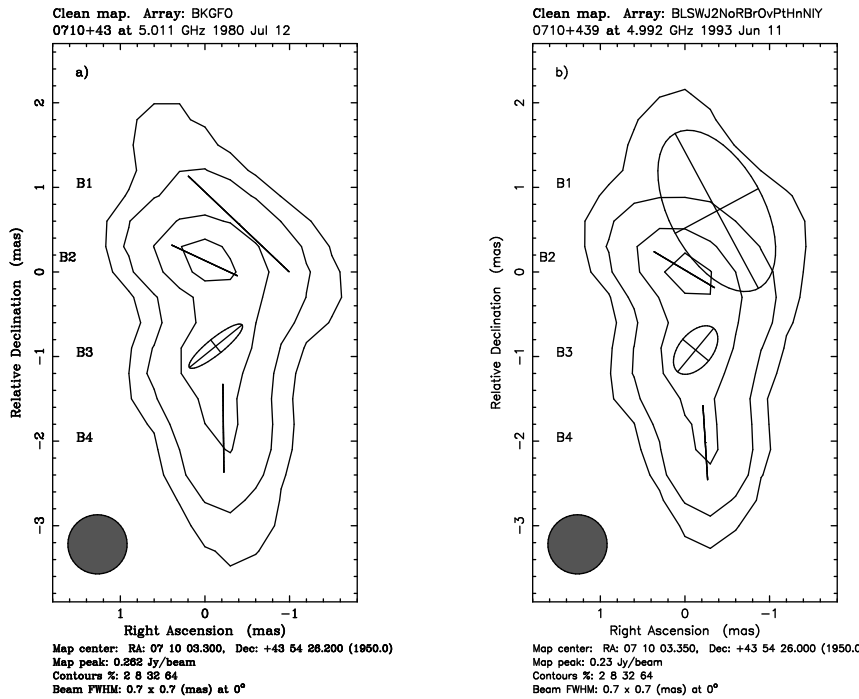


Fig. 2. Modelfit gaussians within middle component of 0710+439 at 5 GHz convolved with a 0.7 mas restoring beam. (a)First epoch; (b)Fifth epoch

Finally the u - v data were amplitude self-calibrated against the model and one final iteration of modelfitting carried out in which component positions were again allowed to vary. We note that it was never necessary at any epoch to change the size or shape of the gaussians within the A or C components. The final models had good agreement factors to the data (for epochs 1 to 5 total agreement factors were $Q_{TOT}=1.149$, $Q_{TOT}=1.047$, $Q_{TOT}=1.039$, $Q_{TOT}=1.145$ and $Q_{TOT}=1.224$ respectively).

4.2. Component Position and Flux Variations

From the modelfits we measured the separation of many pairs of components as a function of time and fitted linear regression lines to this data to estimate relative velocities (see Table 3, Fig. 3).

Although in VLBI data analysis various attempts have been made to estimate *a priori* error bars on component positions these schemes are of doubtful reliability. Gaussian error bars estimated from the variability of reduced Chi-squared on moving the components critically depend on the number of degrees of freedom in the data which depends in turn on the unknown degree of correlation of phase and amplitude errors with time. In addition as noted in section 4.1 even our best fitting model has a reduced Chi-squared which is much further from unity than would be expected given statistical arguments. Given this situation we chose instead to estimate errors on motions from the internal scatter of our data. In addition tests of sig-

nificance of apparent motions were made using standard methods of linear regression analysis. These methods applied to our data suggest that for the brighter components the random errors on the relative separation in each epoch are of order $20\mu\text{as}$. This is comparable to the estimates we obtained from imaging simulations (See Appendix A2).

We find from our fitting that there is no evidence for relative motion between any of the components A1, A3, B1, B2, B4, C1 and C2 (we will refer to these components as the ‘stationary’ group). In contrast the most significant separation we find is between the outer components A2 and C2. From linear regression analysis of MODELFIT data we find a separation rate between these two components of $14.116 \pm 1.604 \mu\text{as yr}^{-1}$ (see Fig. 3). These components are well separated on our CLEAN images which allows us to also use the AIPS task JMFIT to fit the position of A2 and C2 on the CLEAN images at each epoch, giving a similar separation rate of $15.538 \pm 0.445 \mu\text{as yr}^{-1}$.

Given the small number of degrees of freedom tests of significance are best made from examining the correlation coefficients obtained from our linear regression analysis. For the MODELFIT and JMFIT analysis of the A2-C2 separation we obtain correlation coefficients between epoch and separation of 0.981 and 0.998 respectively, which allows us to reject the null hypothesis of no motion at better than the 1% and 0.1% confidence levels. Analysis of other pairs of components (see Table 3) suggests that the significant change in A2-C2 separation is caused primarily by motion of A2 Northward rather than

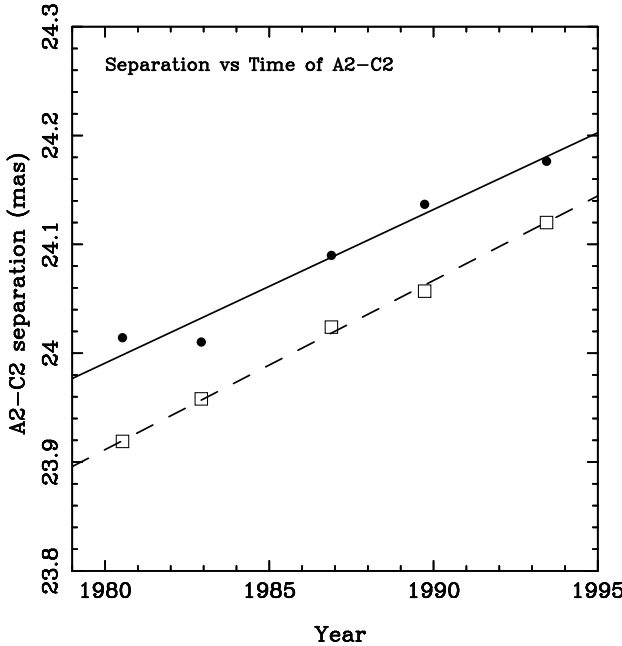


Fig. 3. Changes in separation with time of the components A2 and C2. Circles represent data obtained by MODELFIT, solid line shows linear regression fit to these data. Open squares represent data obtained by JMFIT, dashed line shows linear regression fit. See Section 4.3 for a discussion of the errors on the plotted points and the fits.

motion of C2 Southward. For instance we found the separation of A2-B2 to be $12.913 \pm 2.555 \mu\text{as yr}^{-1}$, very similar to the A2-C2 separation. In contrast the B2-C2 separation of $0.0014 \pm 0.0034 \mu\text{as yr}^{-1}$ is consistent with zero.

Amongst the other components the only other indication of motion is that B3 is moving northward relative to B2 (and B4 and other members of the stationary group) at a rate of $6.089 \pm 1.752 \mu\text{as yr}^{-1}$. We also searched for motions between component pairs in directions perpendicular to the vectors separating them but found no significant motions.

Finally in our analysis of the multi-epoch data we searched for variations in component flux densities. In order to eliminate the effects of errors on the overall flux density scale at each epoch we measured the ratio of each component flux to that of component C2. None of the ‘stationary’ components showed significant flux variations relative to each other or to C2, strongly arguing that all these components stayed constant in flux density over the observing period. We did however detect strong variability of the flux ratio for A2/C2 (see Fig. 4), implying changes in the A2 flux density and also a possible steady increase in the flux density of B3 of about $24\% \pm 8\%$ between the first and the last epochs.

Table 3. Measured apparent motion of the components (MODELFIT) of 0710+439

Components	Apparent velocity [$h^{-1}c$]	Error
A2-A1	0.17367	0.21269
A2-A3	0.16312	0.05612
A2-B2	0.22366	0.04425
A2-B4	0.25035	0.10929
A2-C2	0.24449	0.02782
B2-B1	0.18827	0.15876
B2-B3	-0.10546	0.03035
B2-B4	0.03057	0.06642
B2-C2	0.02373	0.05859
C1-C2	-0.34234	0.24605

4.3. Bulk Motion or Internal Structure Changes?

The change in separation of the outer components of 0710+439 over 13 years is approximately 1/7 of the beam FWHM in the North-South direction. However we note that this shift is 1/3 of the FWHM of the A2 component in the same direction. This large shift combined with the fact that it appears to be consistent from epoch to epoch (see Fig. 3) and is the same when measured relative to several gaussian components, strongly argues that the motion of component A2 is real.

One possibility that must be eliminated is that the apparent change in the centroid position of A2 is not due to motion of the whole component Northward but instead is due to changes in its internal structure. There could for instance be changes of the relative flux density of stationary subcomponents within A2. However the non-monotonic change of the total flux density of A2 (see Fig. 4) seems to be inconsistent with a linear change of the centroid position of A2 (see Fig. 3). It also seems unlikely that if there were two subcomponents within A2 separated by a large enough distance to explain the detected centroid shift that we could still get a good fit at every epoch with a single gaussian component. Furthermore we would expect to see changes in the apparent size of the component with epoch which we do not see. Another possibility is that A2 consists internally of a true stationary hotspot and a jet knot which moves toward it. Again in this case we would have difficulty fitting A2 with a single gaussian and would expect to see the width of the whole component becoming smaller with time, which we do not see. While it is always possible to construct ‘Christmas Tree’ models in which the brightening and dimming of stationary components mimics bulk motion (Scheuer 1984), such models would need to be contrived to fit the observed changes in 0710+439.

We argue that the changes seen are instead due to bulk motion of A2.

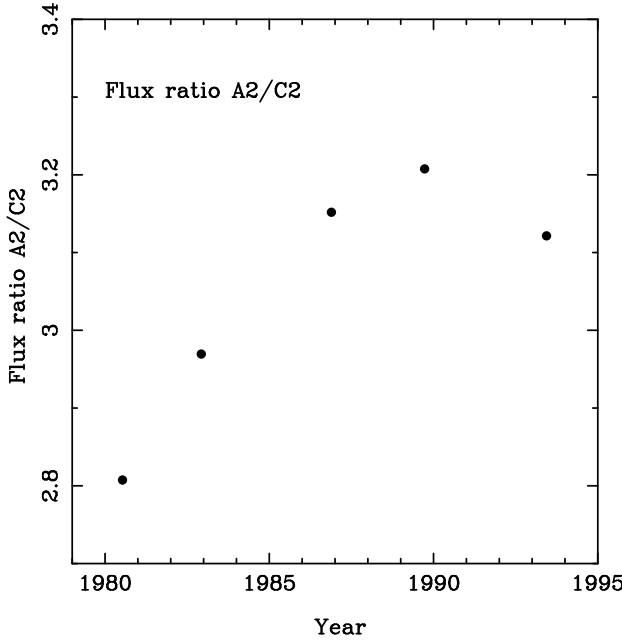


Fig. 4. Measurements of the flux density ratio of A2 and C2 components as a function of time

4.4. Motions Relative to the Core

Our analysis of the component motions showed (see Section 4.2) a group of components (A1, A3, B2, B4, C1, C2) which are stationary relative to each other. Because we were not able to detect the core position in our maps or models (except tentatively in the 5th epoch, see Section 3.3), we do not know for certain the motion, if any, of these components relative to the core.

However it seems most likely that this group is stationary relative to the core and define a rest frame. If this is not the case than all these components, on different sides of the source, must move in unison, in a coordinated way relative to the core; a situation which appears very unlikely. Consider for instance if component C2 and hence the rest of the stationary group moves Southward from the core at $0.122 h^{-1}c$ (exactly half of the A2-C2 separation rate). This scenario has the advantage that both A2 and C2 components are then advancing away from the core at the same speed. But in this case features B2 and B4 would be moving Southward *towards* the core at of $0.122 h^{-1}c$. Since we believe that B2 and B4 are jet features the probability that both would be moving inward toward the core at the same speed, with an amplitude exactly matching the advance speed of A2 and C2 outward, would seem to be very low. The stationary group of components might conceivably move Northward, but than component

C2 would be moving inwards to the core, which seems to be unphysical if C2 is, as we expect, the Southern hotspot.

We conclude that the most likely scenario is that all the components in the ‘stationary group’ are also stationary with respect to the core as well as with respect to each other. In this case B2 and B4 are naturally interpreted as stationary shocks within the jet, and B3 as a possible travelling shock moving outward along the jet at $0.1h^{-1}c$ (see Section 4.2). However a consequence of this model is that the advance speeds of the two outer components, A2 and C2 through the surrounding medium are likely to be different. Consider the separation rates of A2-B2 and C2-B2, which give the lowest estimated errors (see Table 3) of A2 and C2 motion relative to a stationary component. From these measurements we estimate an advance speed for A2 of $0.224 \pm 0.044 h^{-1}c$ and for C2 $0.024 \pm 0.059 h^{-1}c$. If jet component B2 has after all a small undetected velocity outward relative to the core then the implied asymmetry in the advance speeds of A2 and C2 relative to the core would be increased. We note however that despite the apparent velocity difference statistical tests can only exclude the null hypothesis of no difference between the A2-B2 and C2-B2 advance speeds at the 10% confidence level. Therefore this result must be confirmed by future observations.

5. Discussion

5.1. Hot spot Advance Speeds and Source Age

The fact that the A2 and C2 gaussian components are compact and lie at the leading edges of the minilobe emission strongly argues that they should be interpreted as hotspots where two oppositely directed jets terminate (see Fig. 1a,b). In section 4.2 we considered the relative separation rates of the different components of 0710+439, and found the highest significance detection to be that of the separation rate of A2-C2 of $0.2445 \pm 0.0278 h^{-1}c$. Given the overall projected size of 0710+439 this separation velocity gives an age (corresponding to the time when A2-C2 were coincident) of 1400 ± 150 yrs, implying that 0710+439 is a very young radio source. One complication however that must be considered is that, as discussed in Section 4.4, the hotspot advance speeds of A2 and C2 may be different.

In 0710+439 as in other CSO’s the distances from the two hot spots to the core are very similar, i.e. the ratio of these distances (the ‘arm length ratio’) is only 0.95 (Readhead et al. 1996c). This implies the mean advance speeds of the two hotspots averaged over the history of the source have been the same. This fact must be reconciled with the probability of different instantaneous advance speeds for A2 and C2 at the present epoch. One obvious explanation is that C2 is presently interacting with a NLR cloud while A2 advances rapidly through the intercloud medium. If around 100 such clouds have been encountered by each hotspot there would be enough cloud encounters to ex-

plain an arm length ratio close to unity, yet few enough to explain the constant velocity of A2 over 13 years.

Assuming that A2 is close to its equipartition pressure (supported by the analysis of the frequency of its Synchrotron Self Absorbed turnover, Conway et al. 1992) and that the source is orientated not too far from the sky plane then ram pressure arguments imply an external density of $2.8 h^{18/7} \text{ cm}^{-3}$. This value is similar to that estimated in the CSO 2352+495 ($3 - 10 \text{ cm}^{-3}$, Readhead etc al. 1996a) and is consistent with what is expected for the NLR intercloud medium. In contrast estimates of the density encountered by C2 critically depends on its exact advance speed. The observational limits for the C2 advance speed ($0.024 \pm 0.059 h^{-1} \text{c}$) are consistent with an arbitrarily small value and hence ram pressure confinement by an arbitrarily large density as might be expected in a cloud. On the other hand at the upper end of the allowed range of advance speeds the required density could equal that for A2. In this latter case no cloud would be required to explain the lower advance speed of C2; its lower advance be simply a consequence its lower pressure. Since the equipartition pressure of C2 is 0.3 of A2, the expected advance speed for the same external density is 0.55 of A2, given the A2-C2 separation rate this implies a C2 advance speed of $0.086 h^{-1} \pm 0.010 h^{-1} \text{c}$, which is within 1σ of the observed B2-C2 separation rate.

Three-dimensional numerical simulations of advancing jets in a uniform medium (Norman 1996) show strong time variations in the rate of hotspot advance due to variations in hotspot pressure similar to those seen on comparing A2 and C2. Hot spot pressure and velocity variations arise due to the effects of vortex shedding and cocoon turbulence acting on the incoming jet which in turn effect the jet collimation and hence the area over which the thrust of the jet is deposited. The simulations predict variations in hotspot advance speed of order of a factor of 2, similar to those required to explain the observations of 0710+439; it therefore does not seem necessary to postulate cloud interactions to explain our observations. The hydrodynamic explanation also naturally explains why the slower moving hotspot in 0710+439 has lower pressure. In contrast if C2 were embedded within a dense cloud one might expect its pressure to *increase* in response to the higher density.

From the above discussion it seems likely that at present the Northern hotspot (A2) is advancing somewhat faster than its average advance speed and the Southern hotspot (C2) somewhat less. Comparisons with hydrodynamic simulations (Norman 1996) show that the present advance rates of A2 and C2 must be close to their maximum and minimum values respectively and so the measured separation rate ($0.244 \pm 0.028 h^{-1} \text{c}$) will approximately equal the mean separation rate. The mean projected advance speed of each hotspot through the surrounding medium is therefore $0.122 \pm 0.014 h^{-1} \text{c}$. Given the overall size of 0710+439 we therefore again estimate an age of 1400 ± 150 yr. If cloud collisions are instead

the reason for hotspot speed variations, the age estimate is more uncertain and depends inversely on the fraction of time, f , the hotspots spend transversing the intercloud medium. We can argue that since we apparently detect such an advance in the first CSO for which we have more than a decade of monitoring f is unlikely to be less than 0.1, and so we obtain an upper age limit of 14,000 yrs.

Since CSO's are dominated by unbeam emission we expect for a sample selected on total flux density that the angle between the jet axis and the sky plane is about 30° . Such an orientation for 0710+439 is compatible with the hotspots appearing at the extreme ends of the radio emission and not superimposed on the diffuse minilobe emission as we would expect for an end-on source. We therefore expect the mean hotspot advance speed through the external medium to be only slightly larger than that measured for the mean projected advance speed (i.e. $0.122 h^{-1} \text{c}$).

Given our age estimates and estimates of the jet thrust (Readhead at el. 1996a) we can compare the mechanical luminosity required to drive the hot spots forward with the radio luminosity and jet power. For an age of 1400 yrs the combined mechanical luminosity of the two hot spots is $0.6 \times 10^{44} h^{-17/7} \text{ erg s}^{-1}$, while the radio luminosity of the two hotspots is about $0.5 \times 10^{44} h^{-2} \text{ erg s}^{-1}$. Following the arguments used in Readhead et al. (1996a) from the measured hotspot sizes and pressures the upper limit on the total power supplied by the jets is $7.7 \times 10^{44} h^{-10/7} \text{ erg s}^{-1}$. A lower limit on the total jet power can be obtained by adding together the radio power and mechanical work. The total jet luminosity is (for $h=0.6$) therefore in the range $3.5 \times 10^{44} \text{ erg s}^{-1}$ to $16.1 \times 10^{44} \text{ erg s}^{-1}$ and the efficiency of conversion of jet energy to radio emission is between 9% and 41%. In contrast for classical FRII radio galaxies we estimate upper limits on hotspot radiative efficiencies of a few percent by comparing total radio luminosities to estimates of the jet luminosities given by Rawlings & Sanders (1991).

5.2. Implications for CSO Models

Our estimates for the mean hotspot advance speeds in 0710+439, i.e $0.12 h^{-1} \text{c}$, are somewhat larger than those estimated by other authors for the CSO population in general (e.g. Readhead et al. 1996b estimates 0.02c). One would expect a range in properties from CSO to CSO and it might be the 0710+439 lies at the extreme end of the population. However, Conway et al. (1994) tentatively detected, based on two global 5GHz epochs, mean hot spot advance velocities of $0.09 h^{-1} \text{c}$ and $0.065 h^{-1} \text{c}$ in 0108+388 and 2021+614 respectively (the identification of 0108+388 as a CSO is certain, that of 2021+614 less so; Conway et al. 1994). In addition for the CSO 2352+495 Readhead et al. (1996a) gives age estimates of 1200 - 1800 yrs based on synchrotron ageing and 1500 - 7500 yrs from energy supply arguments. For this source of size $120 h^{-1} \text{pc}$ an age

near the lower end of the allowed range, i.e. 1500 yrs gives a mean hotspot advance speed of $0.13h^{-1}c$.

The lower estimates of hotspot advance speeds for the CSO population in general ($0.02c$) made by Readhead et al. (1996a) were based on a two part argument, namely: i) it was argued that hotspot pressures adjusted to the external density so that hotspot advance speeds are constant. Therefore advance speeds of high pressure hotspots in young sources transversing the dense ISM are the same as in the classical double sources ii) Classical double sources, based primarily on observations of Cygnus A, have advance speeds of $0.02c$.

The first part of the above argument was based on detailed observations of three CSO's, in which the arm-length ratios are close to one and therefore the mean advance speeds for the two hotspots must be the same, despite in each case the pressures of the two hotspots being quite different. Readhead et al. (1996b) explicitly assumed that the characteristics of the hotspots are constant in time and that the pressure ratios measured now are typical of the whole history of these sources. It follows that hotspot advance speeds must be independent of hotspot pressure. It was postulated that this could be achieved if a mechanism existed where the hotspot pressure always adjusted to the external density so that ram pressure balance gave a constant advance speed.

In contrast 3-D numerical simulations (Norman 1996) indicate that due to hydrodynamic effects individual hotspots can rapidly vary their pressures around some mean value as they move outward. Differences in pressures between hotspots seen in maps may therefore be just temporary features of sources. Arm length ratios close to one are simply explained if external densities and mean hotspot pressures on each side of the source are the same, so that mean advance speeds are the same. It follows that no special mechanism is required which adjusts hotspot pressure to external density in order to explain the observations. The main motivation which led Readhead et al. (1996b) to propose a universal constant hotspot advance speed for both CSO's and classical sources is therefore removed.

In contrast to Readhead et al.'s (1996b) observational approach Begelman (1996) has calculated the evolution expected for a simple theoretical model of a source with an over-pressurised cocoon and a hotspot whose mean pressure is a fixed ratio to that of the cocoon. In this model the advance speed depends on the density versus distance of the external medium $\rho \propto r^{-n}$, such that the advance speed $v_h \propto l^\beta$ where l is the source size and $\beta = (n-2)/3$. For n in the plausible range 1.5 to 2.0, then β is in the range -0.17 to 0.0 . It is therefore possible that hotspot advance speeds in CSO's are somewhat faster than in classical sources. Since CSO's are 1000 times smaller than classical sources if n were 1.5, we expect advance speeds which are about 3 times faster.

Readhead et al. (1996a) estimated advance speeds in classical sources to be $0.02c$, mainly based on Cygnus A results. However it appears that Cygnus A is an unusual source in that it lies in an unusually dense environment (Barthel 1996, Reynolds & Fabian 1996). In other FRII's external densities are roughly 30 times smaller (Rawlings & Saunders 1991) yet hotspot pressures are only 3 times smaller (Readhead et al. 1996b), therefore typical ram pressure advance speeds in classical sources might be $0.06c$. Estimates of advance speeds using the size and spectral age of typical FRII's (Rawlings & Saunders 1991) also indicate higher advance speeds of $0.108 \pm 0.098h^{-4/7}c$. Combining a typical FRII advance speed of $0.05 - 0.10h^{-1}c$ with the probable weak evolution of hotspot advance speeds with source size we find that mean hot spot advance speeds in CSO's can plausibly be $0.12h^{-1}c$ or larger.

We conclude that the size of the measured hotspot speed in 0710+439 is compatible with the predictions of theoretical models. Such fast speeds imply that sources have only a short lifetime in the CSO phase. The fact that up to 10% of sources in flux limited samples at 5GHz are CSO's therefore means either that i) not all CSO's evolve into classical sources; some exhaust their fuel before reaching 100kpc size (Readhead et al. 1994) or ii) there is strong luminosity evolution in their radio emission. We favour the second explanation, strong luminosity evolution of the required amount to explain the source size distribution is in fact predicted by the theoretical models. For instance the Begelman (1996) model predicts a radio luminosity proportional to approximately $l^{-0.5}$ assuming a constant jet mechanical power. For the weakly evolving hotspot advance velocity predicted for an external density of the form $\rho \propto r^{-1.5}$, the predicted number of sources in each decade of size then exactly matches the observations (Begelman 1996). As first noted by Readhead et al. (1996a) for 2352+495, and as we find for 0710+439 (see Section 5.1), the limits on the radiative efficiency for CSO's compared to classical sources empirically demonstrate that the expected luminosity evolution does in fact occur and with a magnitude (a factor of 30 from CSO to classical sources) consistent with that expected by theory. Given this efficiency evolution one would expect 0710+439 to evolve into a source of radio luminosity $2 \times 10^{42}h^{-2}$ erg s^{-1} , i.e. a weak FRII. We conclude that CSO's are a youthful stage in the evolution of powerful extragalactic radio sources and that these sources most probably evolve into lower luminosity FRII classical radio sources.

Acknowledgements. We thank the observatories of the US and European VLBI Networks and NRAO, which operates the VLA and the VLBA. NRAO is operated by Associated Universities, Inc., under cooperative agreement with the National Science Foundation.

I. Owsianik acknowledges support from the Polish State Committee for Scientific Research grant nr 2.P304.003.07, EU grant (ERBCIPDCT940087) and Onsala Space Observatory.

A. Appendix

We must be careful with the interpretation of multi-epoch data, because analysis methods can strongly affect the reliability of our results. It is very important to know what features to believe, and how accurate our measurements of very small changes are. To investigate these problems we made mapping and modelfitting tests in which we generated simulated data using the program FAKE in the Caltech VLBI data analysis package with the same u - v coverages as the real observations. These ‘fake’ data contained realistic additive Gaussian noise, random antenna-based phase errors and time-varying amplitude calibration errors of order of 10%.

A.1. Reliability of features in CLEAN maps

Fake data for the 1st and 5th epoch were made using the same 9 gaussian components model, which was fitted to the real 5th epoch data (see Table 2). These simulated data were each mapped separately with a point component as a starting model. The final maps had different extended structures in the Northern and Southern components, they also contained apparent bridge emission between these three main components, which was not part of the model. These detected errors were presumably due to inadequacies and differences in u - v coverage at each epoch combined with differences in the details of mapping at each ‘fake’ epoch (choice of windows etc). This test leads us to the conclusion that the details of diffuse and bridge structures seen in the CLEAN maps made from real data (see Fig. 1a) are not reliable. We also conclude that using maps made separately at each epoch is an unreliable way of detecting changes in source structure.

A.2. Estimating modelfitting component position errors

As described in Section 4.1 we can set accurate limits on motion by gaussian modelfitting to each epoch. We carried out ‘fake’ simulations to answer two questions about this procedure. The first was to determine the size of the remaining random errors due to different u - v coverages at each epoch under the null hypothesis of no component motion. The second question was to investigate if this method introduced systematic errors by biasing the results in the sense that real changes would be removed or reduced by initially trying to force the data at each epoch to agree with the same 5th epoch starting model.

In the first test we make our simulations as realistic as possible, we attempted to take account of fact that the real source structure in 0710+439 is almost certainly more complex than can be represented by only 9 Gaussian components. This complexity is demonstrated by the fact the final agreement factors (see Section 4.1) of our models are further from unity than would be expected purely from random noise. It is conceivable that this extra complexity might interact with differences in u - v coverage to give

apparent changes in the centroid position when a 9 component model is fitted at each epoch, even if no position changes actually occur in the source. To test the above possibility we created a 18 component model by replacing each component in the original 9 component model by two slightly shifted gaussians. The final model was such that the agreement factors on fitting a 9 component model to the corresponding ‘fake’ data was roughly similar to that obtained with the real data.

Having chosen a suitable 18 component model we created ‘fake’ data for the 1st and 5th epochs. Using a procedure as similar as possible to that used to analyse the real data we then fitted a 9 component model at each epoch and compared the separations between the gaussians we obtained. The size of the apparent changes gave us an estimate of the residual random error. On doing this test we found an apparent change of A2-C2 separation of 8.09 μ as and in the A2-B2 separation of 30.9 μ as between 1st and 5th epoch. The values are much smaller than the changes in component separation which we detected from the real data (see Fig. 3) and comparable with the variances we estimated from linear regression (see Section 4.2).

A.3. Biasing due to cross self-calibration

In our final test we sought to determine if our modelfitting procedure introduced a systematic error due to initially self-calibrating all models against the same 5th epoch starting model. It is possible that real changes might be reduced or removed by initially trying to force all epochs to agree with the 5th epoch model. To quantify this effect we simulated the case of a 200 μ as shift of A2 (and then C2) position between epochs 1 and 5. Applying our standard modelfitting procedure (see Section 4.1) we determined an estimated motion of just under 200 μ as. The largest negative bias found in our test was only 9 μ as. We conclude that this biasing mechanism has a negligible effect on the estimate in the shift of A2 seen in the real data.

References

Aller, M.F., Aller, H.D., Hughes, P.A., 1992, ApJ, 399, 16
 Barthel P.D. & Arnaud K.A., 1996, MNRAS, 283, L45
 van Breugel W.J.M., Heckman T.A., Miley G.K., 1984, AJ, 89, 5
 Begelman M.C., 1996, Cygnus A-study of Radio Galaxy. In: Proc. of the Greenbank Workshop, Carilli C.L, Harris D.E. (eds.), CUP, Cambridge, p.209
 Clark B.G., 1973, Proc IEEE, 61, 1242
 Cohen M.H., 1975, ApJ, 201, 249
 Conway J.E., Pearson T.J., Readhead, A.C.S., Unwin S.C., Xu W., Mutel R.L, 1992, ApJ, 396, 62
 Conway J.E., Pearson T.J., Readhead A.C.S., Unwin S.C., Xu W., 1994, ApJ, 425, 568
 Fanaroff B.L., Riley J.M., 1974, MNRAS, 167, 31P
 Fanti C., Fanti R., Dallacasa D., Schilizzi R.T., Spencer R.E., Stanghellini C., 1995, A & A, 302, 317

Henstock D.R., Browne I.W.A., Wilkinson P.N., Taylor G.B., Vermuelen R.C., Pearson T.J., Readhead A.C.S., 1995, ApJS, 100, 1H

Lawrence C.R., Zucker J.R., Readhead A.C.S., Unwin S.C., Pearson T.J., Xu W., 1996, ApJS, 107, 541L

Norman M.L., 1996, Structure and Dynamics of the 3D Supersonic Jet. In: Energy Transport in Radio Galaxies and Quasars. Hardee A.H., Bridle A.H., Zensus J.A (eds.), ASP, San Francisco, vol.100, p.319

Peacock J.A., Perryman M.A.C., Longair M.S., Gunn J.E., Westphal J.A., 1981, MNRAS, 194, 601

Pearson T.J., 1991, BAAS23, 991

Pearson T.J., Readhead A.C.S., 1988, ApJ, 328, 114

Phillips R.B., Mutel R.L., 1982, A &A, 106, 21

Rawlings S., Saunders R., 1991, Nature, 349, 138

Readhead A.C.S., Xu W., Pearson T.J., Wilkinson P.N., Polatidis A.G., 1994, Compact Extragalactic Radio Source. In: Proc. of a workshop, Zensus J.A., Kellermann K.I. (eds.), NRAO, p.17

Readhead A.C.S., Taylor G.B., Pearson T.J., Wilkinson P.N., Polatidis A.G., 1996a, ApJ, 460, 612

Readhead A.C.S., Taylor G.B., Pearson T.J., Wilkinson P.N., 1996, ApJb, 460, 634

Readhead A.C.S., Pearson T.J., Taylor G.B., Wilkinson P.N., 1996c, The Jet Advance Speed in Compact Symmetric Objects. In: Energy Transport in Radio Galaxies and Quasars. Hardee P.E., Bridle A.H., Zensus J.A. (eds.), ASP, San Francisco, vol.100, p.79

Reynolds C.S., Fabian A.C., 1996, MNRAS, 278, 479

Schwab F.R., Cotton W.D., 1983, AJ88, 688

Shepherd M.C., Pearson T.J., Taylor G.B., 1994, BAAS26, 987

Shepherd M.C., Pearson T.J., Taylor G.B., 1995, BAAS27, 903

Scheuer P.A.G., 1984, Explanations of Superluminal motion. In :VLBI and Compact Radio Sources, IAU Symp. 110, Fanti R., Kellermann K., and Setti G. (eds.), Reidel, Dordrecht, p.197

Taylor G.B., Readhead A.C.S., Pearson T.J., 1996, ApJ, 98, 33

Wilkinson P.N., Polatidis A.G., Readhead A.C.S., Xu W., Pearson T.J., 1994, ApJ432, L87

Xu W., 1994, Ph.D. Thesis, California Institute of Technology

de Young D.S., 1996, How do CSO's Grow Old? In: The Second Workshop on Gigahertz Peaked Spectrum and Compact Steep Spectrum Radio Sources, Snellen I.A.G., Schilizzi R.T., Röttgering M.J.A., Bremer M.N. (eds.), Leiden, p.275